



Amino-functionalized synthesis of MnO₂-NH₂-GO for catalytic ozonation of cephalexin

Jie Xu^a, Yu Li^a, Mengqian Qian^a, Jian Pan^b, Jia Ding^a, Baohong Guan^{a,*}

^a College of Environmental and Resource Sciences, Zhejiang University, Hangzhou, 310058, China

^b Environmental Technology Innovation Center of Jiande, Hangzhou, 311600, China



ARTICLE INFO

Keywords:

Catalytic ozonation
Graphene oxide
Manganese dioxide
Amino-Functionalization
Cephalexin

ABSTRACT

Catalysts such as MnO₂ always play a critical role in catalytic ozonation, which is applied extensively in water treatment for disinfection, odor removal and organic pollutants degradation. To improve the performance of catalytic ozonation, we design and synthesize a catalyst of amino-functionalized hybrid of MnO₂ and graphene oxide (MnO₂-NH₂-GO) with hydrothermal method, and then use it to catalyze the ozonation of cephalexin (CLX), one of β -lactams antibiotics frequently detected as refractory pollutants in aquatic environment. The MnO₂-NH₂-GO shows much higher catalytic performance than both MnO₂ and MnO₂-GO in the ozonation of CLX, in which the free radicals of $\cdot\text{O}_2^-$ play a dominated role and the Mn³⁺/Mn⁴⁺ acting as active sites react with ozone to promote the formation of $\cdot\text{O}_2^-$ with the help of the enhanced electron transfer facilitated by GO. The MnO₂-NH₂-GO also shows more stable catalytic performance than MnO₂-GO due to the strong covalent bonds bridged by amino to MnO₂ and GO to prevent the decoupling of GO from MnO₂. This work provides a method to design a smart catalyst for ozonation with high catalytic performance and stability.

1. Introduction

Antibiotics are frequently detected in aquatic environment and have a serious threat on aquatic organisms and aquatic products [1,2]. The continuous input of antibiotics into the environment leads to a quick accumulation in water and poses potential and irreversible harm to human beings as the top role of the food chains [3–5]. The antibiotics in aquatic environment come from municipal sewage, hospital sewage, reclaimed wastewater and wastewater discharged from pharmaceuticals industry. Most of them are recognized as refractory pollutants which are recalcitrant to biodegradation [6,7]. It is urgent for us to develop a technology that can efficiently remove or decompose antibiotics in water or wastewater so as to eliminate the danger from these pollutants. The catalytic ozonation is supposed to be a convenient and promising advanced oxidation technology for water treatment, especially for the removal of refractory organic pollutants from water or wastewater [8,9]. The critical point of this technology lies in the catalytic performance, stability and accessibility. Some transition metal oxides such as MnO₂, ZnO, TiO₂ and Fe₃O₄, are preferred catalysts and have been proven to be efficient and practical in catalytic ozonation by facilitating the generation of free radicals to react with organic pollutants [10–13]. Among them, MnO₂ is a widely used catalyst for ozonation in water treatment thanks to its environmental friendliness,

structural stability and facile fabrication [13,14]. However the catalytic performance of MnO₂ cannot meet the need of water treatment for the removal of pharmaceuticals and personal care products (PPCPs) with desirable efficiencies [15,16]. Thus the researchers develop catalysts based on MnO₂, for example, by compositing MnO₂ with Fe₃O₄, supporting MnO₂ onto carbon nanotube or biologically producing MnO_x [17–20]. Graphene rapidly finds its application as a dopant in improving the catalyst performance for ozonation with its unique 2D structure and outstanding electronic conductivity [21–24]. In this regard the hybrids of graphene or graphene oxide (GO) and MnO₂ have been used in catalytic ozonation, in which GO speeds up the electron transfer and thus stimulates more free radicals generation [25,26]. It is known that the performance of a composite catalyst mainly depends on a stable hybrid structure. However the stability of MnO₂-Graphene catalyst, which is essential to the catalyst application in water treatment, has not aroused enough concerns. Some researches reveal that enhanced chemical bonds between graphene and active constituents not only improve the electrochemical performance of composites, but also strengthen the bonding between constituents [27,28].

Herein we design a catalyst by amino-functionalizing the hybrids of MnO₂ and GO, and choose cephalexin, one of β -lactams antibiotics that are widely used to diminish inflammation and kill bacteria, also one of the main antibiotics pollutants existing in aquatic environment [29], as

* Corresponding author.

E-mail address: guanbaohong@zju.edu.cn (B. Guan).

the model pollutant, aiming to develop a smart catalyst for ozonation to efficiently remove antibiotics from water or wastewater.

2. Experimental section

2.1. Reagents and materials

All chemicals were at least of analytical grade except as noted as received without further purification. All solutions were prepared with ultrapure water. CLX was purchased from Shanghai Macklin Biochemical Co., Ltd (China). GO was supplied by China Carbon Valley Technology Group Co., Ltd. (China). HPLC-grade acetonitrile and methyl alcohol (MeOH) were obtained from Sigma-Aldrich (USA). Other chemicals including potassium permanganate ($KMnO_4$), manganese sulfate monohydrate ($MnSO_4 \cdot H_2O$), sodium bicarbonate ($NaHCO_3$), sodium phosphate (Na_3PO_4), potassium iodide (KI), p-benzoquinone (p-BQ), 3-Aminopropyltriethoxysilane, toluene and ethanol were supplied by Sinopharm Chemical Reagent Co. (China).

2.2. Catalysts preparation

2.2.1. MnO_2

MnO_2 was synthesized with hydrothermal method [30]. In a typical synthesis, 5.42 g $MnSO_4 \cdot H_2O$ and 5.04 g $KMnO_4$ were added into 200 mL ultrapure water, followed by an immediate mixing and continuous stirring for 45 min to form a stock solution. The 170 mL of the stock solution was transferred into a 200 mL Teflon-lined stainless steel autoclave, which was subsequently sealed and put into an oven at the temperature of 140 °C. After 12 h, the autoclave was taken out and naturally cooled down to room temperature before the precipitate was filtered. The solid was washed with ultrapure water and rinsed with ethanol for 3 cycles. Finally, the product was harvested after drying in the oven at 60 °C for 12 h.

2.2.2. Amino-functionalized MnO_2 (MnO_2-NH_2)

Amino modified MnO_2 was fabricated with organosilane and toluene [31]. The prepared MnO_2 was dispersed in 50 ml toluene at 80 °C. After stirring for 0.5 h, 5 ml of 3-Aminopropyltriethoxysilane was added into the mixture to functionalize MnO_2 . After stirring for 12 h, the product of amino-modified MnO_2 was filtered. The solid was washed with ultrapure water and rinsed with ethanol for 3 cycles, and then dried at 60 °C for 12 h.

2.2.3. MnO_2 hybrid with GO (MnO_2-GO)

MnO_2 -GO was synthesized with hydrothermal method. First, 5.42 g $MnSO_4 \cdot H_2O$ and 5.04 g $KMnO_4$ were added into 190 mL ultrapure water to prepare mixed solution under stirring for 45 min, and 0.05 g GO was ultrasonically dispersed in 10 mL ultrapure water in a small serum bottle for 1 h. The GO suspension was added into the mixed solution under stirring for another 30 min to form a stock mixture. Then 170 mL of the stock mixture was transferred into a 200 mL Teflon-lined stainless steel autoclave for hydrothermal synthesis at 140 °C for 12 h. The precipitate was filtered and washed with ultrapure water and rinsed with ethanol for 3 cycles. Finally, the product was harvested after drying in the oven at 60 °C for 12 h.

2.2.4. Amino-functionalized MnO_2 hybrid with GO (MnO_2-NH_2-GO)

To synthesize MnO_2-NH_2-GO , the prepared MnO_2-NH_2 was added into 190 mL ultrapure water under stirring for 45 min, and 0.05 g GO was ultrasonically dispersed in 10 mL ultrapure water in a small serum bottle for 1 h. Then two suspensions are mixed under stirring for 30 min. After that, 170 mL of the mixture was transferred into a 200 mL Teflon-lined stainless steel autoclave for hydrothermal synthesis at 140 °C for 12 h. The precipitate was filtered and washed with ultrapure water and rinsed with ethanol for 3 cycles. The product was harvested after drying in the oven at 60 °C for 12 h.

2.3. Characterization

The crystal phases of as-prepared catalysts were detected by a XRD analyzer (Bruker, Germany) with Cu K α radiation ($k = 1.5418 \text{ \AA}$) at 40 kV and 30 mA with scanning rate of $10^\circ \text{ min}^{-1}$ and 0.02° step in 20 range of 10 - 80°. The infrared spectrum at a range of 400–4000 cm^{-1} with 2 cm^{-1} resolution was determined by a FTIR spectrometer (Thermo Nicolet, Nexus-470, USA) using KBr self-supported pressing technique to analyze the chemical group of catalysts. The X-ray photoelectron microscopy (XPS) was conducted on a Thermo Escalab 250 equipped with Al K α X-ray irradiation (1486.6 eV) at 150 W to detect the elemental composition on the surface of catalysts. The morphology of the catalysts was examined by a field scanning electron microscopy (SEM, Hitachi SU-8010, Japan). Electron paramagnetic resonance (EPR) experiments for radical analysis were performed on Bruker A300 spectrometer (Bruker, Germany) with 5, 5 - dimethyl - 1 - pyrroline (DMPO) as spin-trapping agents. The electrochemical tests were performed on CHI 760E electrochemical analyzer (Chenhua Instruments Company, China) using a three-electrode photo electrochemical cell, in which the counter electrode was platinum wire and the reference electrode was the saturated calomel electrode. The indium tin oxide glass ($20 \times 30 \times 1.1 \text{ mm}$, 15Ω) was used to prepare the working electrode. Firstly, the glass was ultrasonically cleaned in ethanol and deionized water, successively. Then this cleaned glass was dried at 70 °C. After that, the adhesive tape was pasted on the conductive surface of the glass and the pasted area was about $1 \times 1 \text{ cm}^2$. Then epoxy ester AB glue was covered on the remained area of the conductive surface. After drying at 70 °C for 12 h, the glue solidified on the surface and the pasted adhesive tape was removed. Thereafter, 0.02 g catalyst sample was dispersed ultrasonically in the solution prepared with 1 mL N, N - dimethylformamide and 20 μL nafion membrane solution for one hour. Finally, 50 μL of the resulted slurry was added dropwise onto the conductive surface ($1 \times 1 \text{ cm}^2$ area) and then dried at 70 °C for 12 h. The electrolyte solution was 0.2 M Na_2SO_4 solution and the electrochemical impedance spectroscopy tests were carried out in darkness.

2.4. Experimental procedures

The batch experiments were conducted open to the air and in a series of borosilicate glass jars containing 200 mL solution at 25 ± 1 °C. The initial concentration of CLX was fixed at 1.0 mg/L. The initial concentration of O_3 (0.12 mg/L) in solution was acquired by bubbling ozone gas for about 10 s. The catalytic ozonation was initiated after the introduction of 25 mg/L catalysts. At each time interval (10 s, 1 min, 2 min, 3 min, 4 min, 5 min), the solution was sampled and filtered through 0.22 μm membrane before analysis.

2.5. Analytical methods

CLX was detected by a high performance-liquid chromatography (HPLC) (Agilent 1260, USA) equipped with a Kromsail C18 column (150 mm, 4.6 mm, 10 μm , Sweden) and a variable wavelength detector (Agilent, USA) at $\lambda = 254 \text{ nm}$. A mixture of 0.015 mol/L CH_3COONa (60%, pH = 4.0), acetonitrile (6%) and methanol (34%) was used as mobile phase at a flow rate of 1.0 mL/min. The injection volume was 50 μL and the retention time of CLX was 2.6 min. The residual concentration of ozone was determined by the indigo method using an UV-Vis spectrophotometer (Pgeneral, TU-1901, China) at $\lambda = 600 \text{ nm}$.

3. Results and discussion

3.1. Performance of catalysts for ozonation

The adsorption of CLX by catalysts in the solution is responsible for less than 3.5% CLX removal (Fig. S1), which is deducted as a background value from the data of CLX concentrations determined under

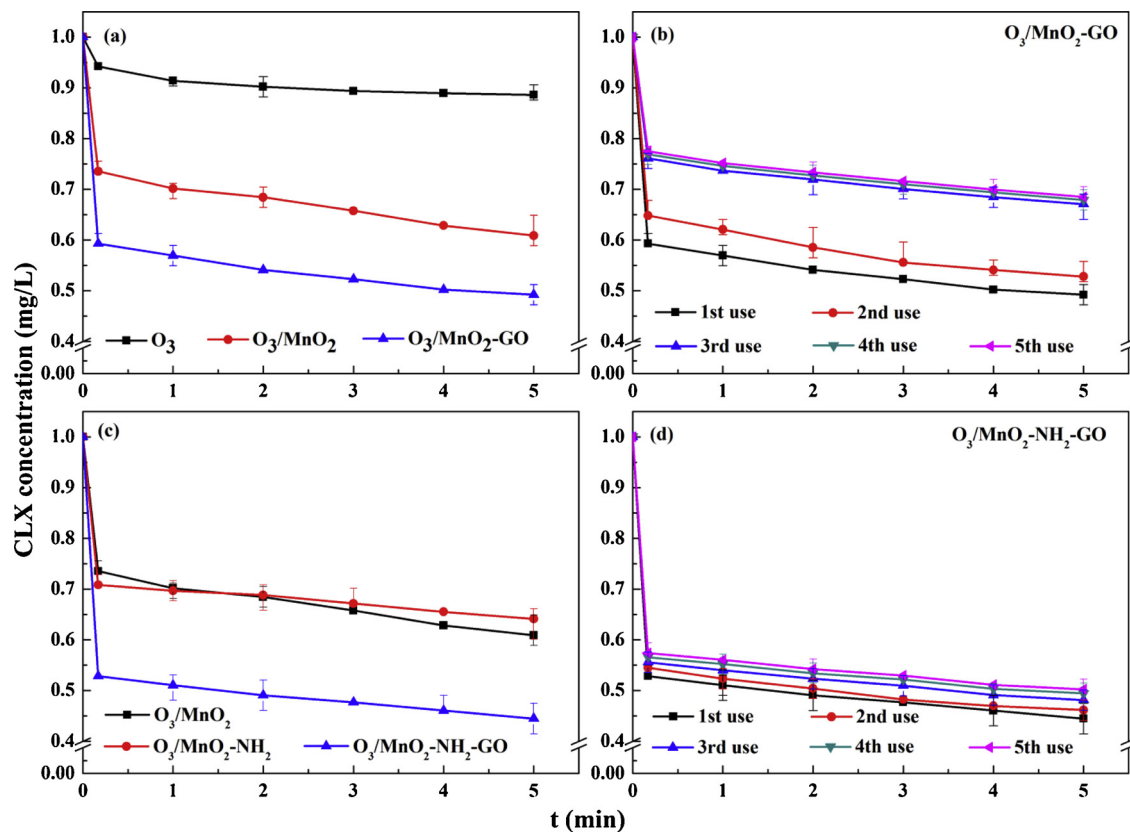


Fig. 1. Cefalexin (CLX) removal by (a) ozonation, catalytic ozonation with MnO_2 or $\text{MnO}_2\text{-GO}$; (b) catalytic ozonation with reused $\text{MnO}_2\text{-GO}$; (c) catalytic ozonation with $\text{MnO}_2\text{-NH}_2$ or $\text{MnO}_2\text{-NH}_2\text{-GO}$; (d) catalytic ozonation with reused $\text{MnO}_2\text{-NH}_2\text{-GO}$. Conditions: $[\text{CLX}]_0 = 1.00 \text{ mg/L}$, catalyst loading = 25 mg/L, $[\text{O}_3]_0 = 0.12 \text{ mg/L}$, and pH = 6.2.

ozonation or catalytic ozonation. Fig. 1a shows the removal of CLX by ozonation (O_3), catalytic ozonation with MnO_2 (O_3/MnO_2) and catalytic ozonation with $\text{MnO}_2\text{-GO}$ ($\text{O}_3/\text{MnO}_2\text{-GO}$) in 5 min. The ozonation removes 11.4% CLX, while O_3/MnO_2 and $\text{O}_3/\text{MnO}_2\text{-GO}$ achieve 38.3% and 50.3% removal efficiency respectively, indicating that the catalytic ozonation by MnO_2 can obtain much higher removal efficiency than ozonation, and GO compositing with MnO_2 to form $\text{MnO}_2\text{-GO}$ dramatically promotes the catalytic ozonation of CLX. By contrast, a dosage of 2.5 mg/L GO, which is the same content of GO in the catalyst of $\text{MnO}_2\text{-GO}$, exhibits very low effect on the removal of CLX by ozonation (Fig. S2).

The stability is another important index to the performance of catalyst. Fig. 1b depicts the CLX removal by catalytic ozonation with reused $\text{MnO}_2\text{-GO}$. The second use, third use, forth use and fifth use of $\text{MnO}_2\text{-GO}$ show the CLX removal decrease from 50.3% to 46.2%, 33.9%, 33.2% and 32.4% in 5 min reaction, respectively, witnessing a gradual decline of $\text{MnO}_2\text{-GO}$ performance for catalytic ozonation. The SEM images of $\text{MnO}_2\text{-GO}$ (Fig. 2a-c) show that the needle-shaped crystals of MnO_2 gradually decouple from the GO particles after second use and third use, leading to a less dense of MnO_2 crystals contacting with GO. Evidently the compositing of GO to MnO_2 improves the catalytic performance, and the stability of the catalyst of $\text{MnO}_2\text{-GO}$ probably depends on the bonding between MnO_2 and GO.

Since MnO_2 crystals combine with GO by physical absorption or electrostatic interaction [32], the weak bonding force cannot resist the shearing force and scouring force from fluid, resulting in a gradually decoupling of MnO_2 crystals from GO during reaction and thus weakening the catalytic performance of $\text{MnO}_2\text{-GO}$. To improve and maintain the stability of $\text{MnO}_2\text{-GO}$, amino-functionalization is employed to bond MnO_2 and GO to form a new structure for catalyst of $\text{MnO}_2\text{-NH}_2\text{-GO}$. The XRD patterns of MnO_2 , $\text{MnO}_2\text{-NH}_2$, $\text{MnO}_2\text{-GO}$ and $\text{MnO}_2\text{-NH}_2\text{-GO}$

are shown in Fig. S3. For all catalysts the crystal phase of MnO_2 is $\alpha\text{-MnO}_2$. The amino-functionalization or the compositing with GO neither changes the phase of MnO_2 nor generates new phase. The XPS spectra of N 1s regions of $\text{MnO}_2\text{-NH}_2\text{-GO}$ shown in Fig S4 prove that $\text{NH}_2\text{-}$ exists on the surface of $\text{MnO}_2\text{-NH}_2\text{-GO}$, indicating the amino functionalization works very well on $\text{MnO}_2\text{-GO}$. The FTIR spectra of GO, MnO_2 , $\text{MnO}_2\text{-NH}_2$, $\text{MnO}_2\text{-GO}$ and $\text{MnO}_2\text{-NH}_2\text{-GO}$ are shown in Fig. S5. The amino functionalization of MnO_2 to form $\text{MnO}_2\text{-NH}_2$ is verified by two amino peaks around 1134 cm^{-1} and 3358 cm^{-1} , symbolized by the bending vibration of N–H bond. $\text{MnO}_2\text{-NH}_2\text{-GO}$ exhibits a different profile of spectrum from that of $\text{MnO}_2\text{-NH}_2$. The characteristic peaks of N–H bond at 1134 cm^{-1} and 3358 cm^{-1} shrink drastically, which convincingly reveal that GO is bonded with amino on the surface of MnO_2 . Both XPS and FTIR shows that the amino-functionalization endows $\text{NH}_2\text{-}$ to MnO_2 to bond with GO for compositing catalyst of $\text{MnO}_2\text{-NH}_2\text{-GO}$.

Fig. 1c shows in 5 min reaction the $\text{O}_3/\text{MnO}_2\text{-NH}_2$ gains 36.9% CLX removal, almost the equal efficiency value to that of O_3/MnO_2 , indicating the amino-functionalization cannot improve the catalytic performance of MnO_2 for ozonation. However the $\text{O}_3/\text{MnO}_2\text{-NH}_2\text{-GO}$ achieves 55.6% CLX removal, much higher than those of $\text{O}_3/\text{MnO}_2\text{-NH}_2$ (36.9%) and $\text{O}_3/\text{MnO}_2\text{-GO}$ (50.3%), implying the amino-functionalization makes a much strong bonding between MnO_2 and GO. Such a strong bonding makes the electrons transfer more forthrightly and fleetly at the time of reaction [33].

Fig. 1d presents the CLX removal by reuse of $\text{MnO}_2\text{-NH}_2\text{-GO}$ for catalytic ozonation. The four times reuse of $\text{MnO}_2\text{-NH}_2\text{-GO}$ exhibits less than 5.0% decrease in CLX removal, while the four times reuse of $\text{MnO}_2\text{-GO}$ shows the CLX removal decreases from 50.3% to 32.9%, demonstrating that the amino-functionalization endows $\text{MnO}_2\text{-NH}_2\text{-GO}$ a stable performance in catalytic ozonation. Fig. 2(d-f) shows that even after the third use the $\text{MnO}_2\text{-NH}_2\text{-GO}$ almost maintains its original

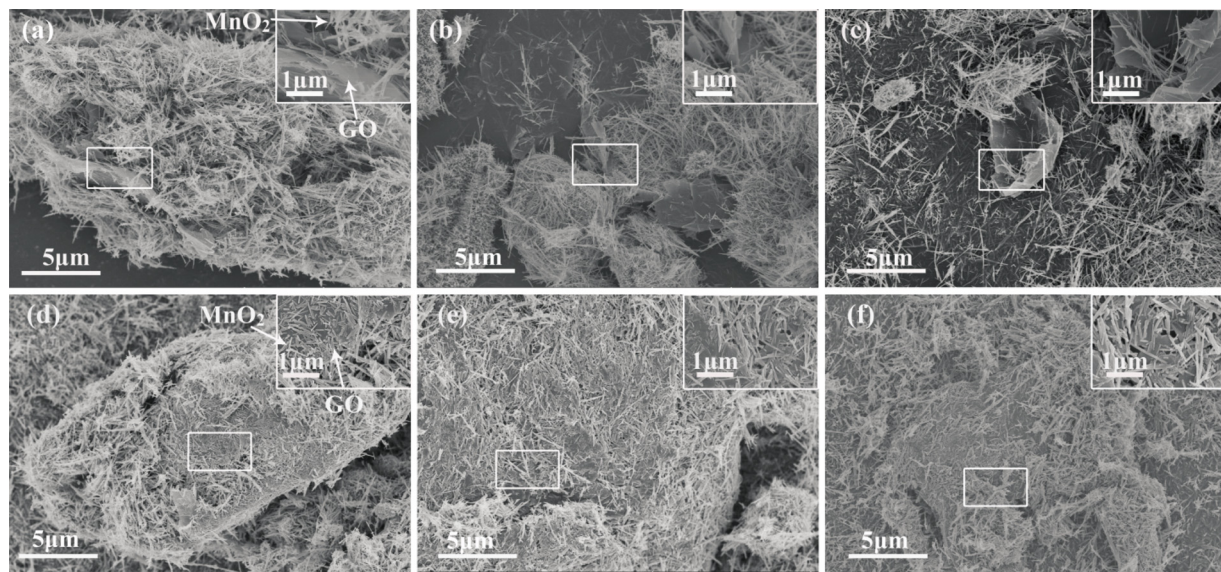


Fig. 2. SEM images of MnO₂-GO at first use (a), second use (b) and third use (c), and MnO₂-NH₂-GO at first use (d), second use (e) and third use (f).

structure with dense MnO₂ crystals attached to GO particles, which implies that the amino-functionalization brings an intensive hybridization of MnO₂ and GO. It can be believed that the amino-functionalization improves the stability of the catalyst by reinforcing the bonding of MnO₂ with GO to prevent their decoupling.

3.2. Effect of amino-functionalization on ESI

GO improves the performance of catalyst by accelerating the electron transfer during the reaction [34,35]. That is, the decoupling of GO from MnO₂-GO or MnO₂-NH₂-GO is certainly to decelerate the electron transfer and thus weaken the performance of catalysts. The electrochemical impedance spectroscopies (EIS) of MnO₂-GO and MnO₂-NH₂-GO are shown in Fig. 3. The Nyquist plots express the charge transfer rate at the interface between the working electrode (made of catalysts) and the electrolyte, in which the arc radius indicates the internal resistance between the electrode and the electrolyte [36,37]. Fig. 3a shows the arc radius of MnO₂-GO Nyquist plot becomes larger and larger after second use and third use, indicating a deactivation between MnO₂ and GO. The arc radii of MnO₂-GO present a significant shifting from first use to fifth use, and the arc radii of the last three times coincide very well in Nyquist plot, which is consistent with the profile of catalytic performance of MnO₂-GO shown in Fig. 1b. On the contrary, the arc radius of

Nyquist plot varies slightly from the first use to the fifth use of MnO₂-NH₂-GO for catalytic ozonation, and the five arc radii almost converge to one point (Fig. 3b). That is, the electronic conductivity of the catalyst keeps pretty stable, suggesting a strong bonding between MnO₂ and GO has been established in MnO₂-NH₂-GO, which ensures a stable performance of MnO₂-NH₂-GO for catalytic ozonation presented in Fig. 1d. The MnO₂-NH₂-GO exhibits smaller arc radii of Nyquist plot than those of MnO₂-GO, indicating the higher electronic conductivity of MnO₂-NH₂-GO, which is in accord with the better performance of MnO₂-NH₂-GO for catalytic ozonation illustrated in Fig. 1c.

3.3. Catalytic ozonation mechanism

It is generally regarded that the radical species play a major role in decomposing the organic pollutants during catalytic ozonation. To explore the radical species produced by catalytic ozonation with MnO₂-NH₂-GO, the bicarbonate and p-benzoquinone (p-BQ) are selected as the scavengers of ·OH and ·O₂⁻, respectively [38–40]. The results of quenching tests are shown in Fig. 4. NaHCO₃ has not any effect on CLX removal rate, while p-BQ dramatically inhibits the catalytic ozonation and decreases the removal efficiency of CLX from 55.6% to 10.7% in 5 min, which is almost equal to the removal efficiency of ozonation without any catalyst, suggesting that ·OH is not responsible for CLX removal but ·O₂⁻ dominates the catalytic ozonation process.

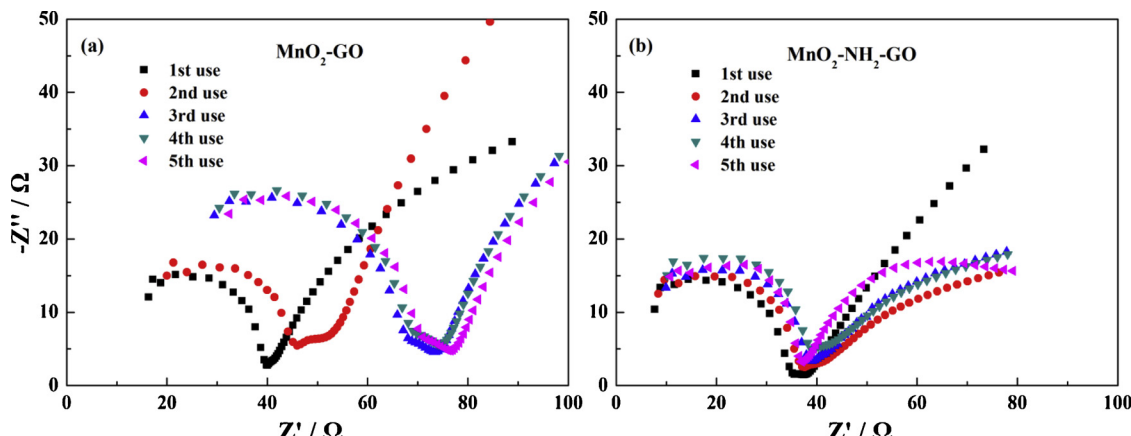


Fig. 3. EIS Nyquist plots of (a) MnO₂-GO and (b) MnO₂-NH₂-GO.

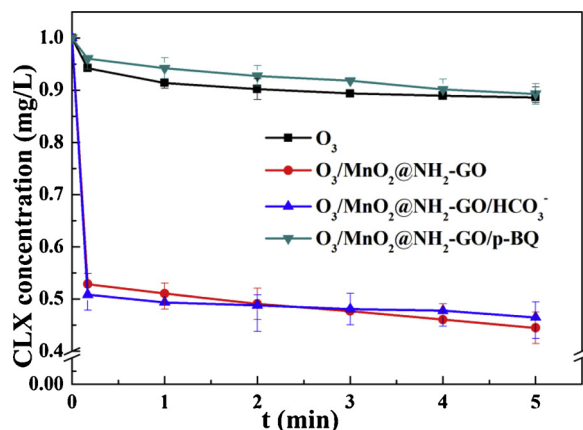


Fig. 4. Influence of radical scavengers on CLX removal by ozonation catalyzed with $\text{MnO}_2\text{-NH}_2\text{-GO}$. Conditions: $[\text{CLX}]_0 = 1.0 \text{ mg/L}$, catalyst loading = 25 mg/L, $[\text{O}_3]_0 = 0.12 \text{ mg/L}$, and pH = 6.2, radical scavengers = 50 mg/L.

To directly elucidate the radical species that formed in the process of ozonation or catalytic ozonation, the EPR experiments were carried out with DMPO as radical spin trapping agents and the results are showed in Fig. 5. The characteristic peaks of both DMPO - $\cdot\text{OH}$ adducts and DMPO - $\cdot\text{O}_2^-$ adducts are not observed in the ozonation, indicating neither $\cdot\text{O}_2^-$ nor $\cdot\text{OH}$ plays a part in the ozonation of CLX. In the catalytic ozonation, the characteristic peaks of DMPO - $\cdot\text{OH}$ adducts do not appear, while the characteristic peaks of DMPO - $\cdot\text{O}_2^-$ adducts emerge strongly, confirming that $\cdot\text{O}_2^-$ rather than $\cdot\text{OH}$ plays a crucial role in the catalytic ozonation with $\text{MnO}_2\text{-NH}_2\text{-GO}$.

The phosphate is employed to investigate the active sites of $\text{MnO}_2\text{-NH}_2\text{-GO}$ due to its strong bonding with the acid sites on the catalyst surface [41,42]. Fig. 6 shows phosphate has a slight positive effect on the ozonation of CLX owing to a slight increase in pH resulted from the added phosphate but a strong suppression on the catalytic ozonation with $\text{MnO}_2\text{-NH}_2\text{-GO}$. The efficiency of CLX removal drops from 55.6% to 17.6%, which is close to that of ozonation without any catalyst. It is inferred that the phosphate occupies the acid sites of the catalyst and thus inhibits the interaction between ozone and the acid sites for the generation of free radicals. The electron transfers occurring at the surface of MnO_2 during catalytic oxidation could be regarded as the acid sites, which should be responsible for ozone decomposition to active radicals.

Fig. 7a-b shows the XPS of Mn 2p region of $\text{MnO}_2\text{-NH}_2\text{-GO}$ in prepared and one time used for catalytic ozonation, where the peaks around 641.7 and 642.7 eV are assigned to Mn^{3+} and Mn^{4+} , respectively [25]. After one time used for catalytic ozonation, the relative content of lattice Mn^{3+} decreases from 53.7% to 47.9% while the

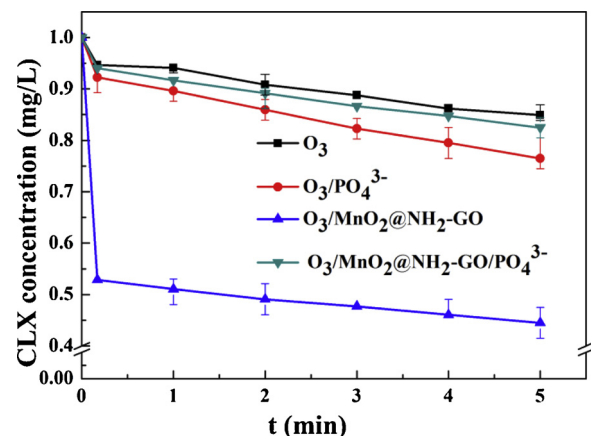


Fig. 6. Influence of phosphate on CLX removal by ozonation catalyzed by $\text{MnO}_2\text{-NH}_2\text{-GO}$. Conditions: $[\text{CLX}]_0 = 1.0 \text{ mg/L}$, catalyst loading = 25 mg/L, $[\text{O}_3]_0 = 0.12 \text{ mg/L}$, and pH = 6.2, phosphate = 50 mg/L.

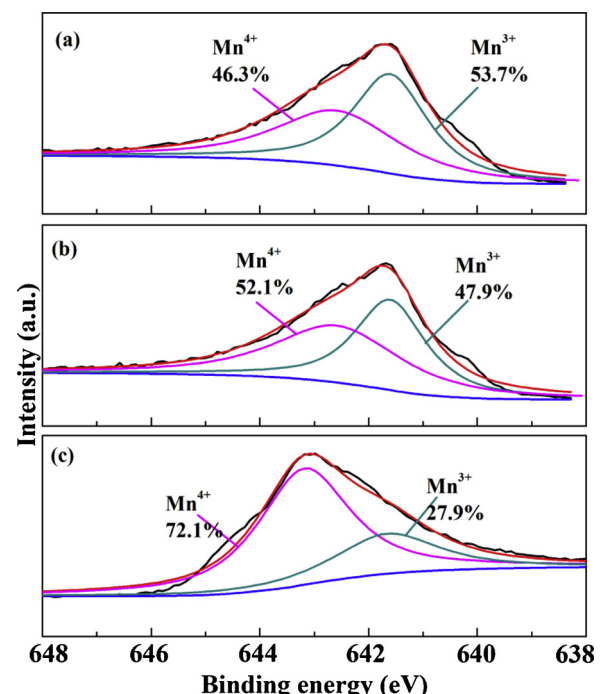


Fig. 7. XPS spectra of Mn 2p regions of $\text{MnO}_2\text{-NH}_2\text{-GO}$ in prepared (a), one time used (b) and five times used (c).

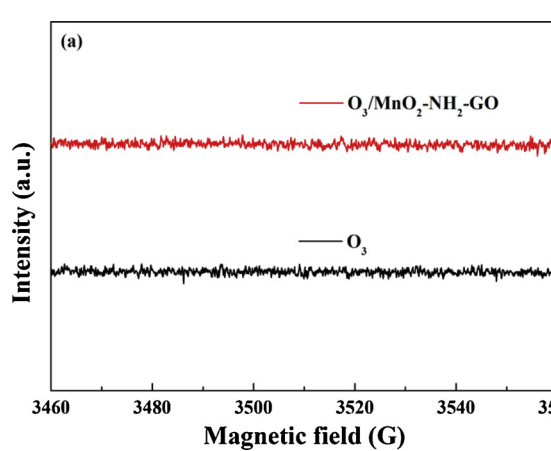


Fig. 5. EPR spectra of O_3 and $\text{O}_3/\text{MnO}_2\text{-NH}_2\text{-GO}$ (a) DMPO - $\cdot\text{OH}$ and (b) DMPO - $\cdot\text{O}_2^-$.

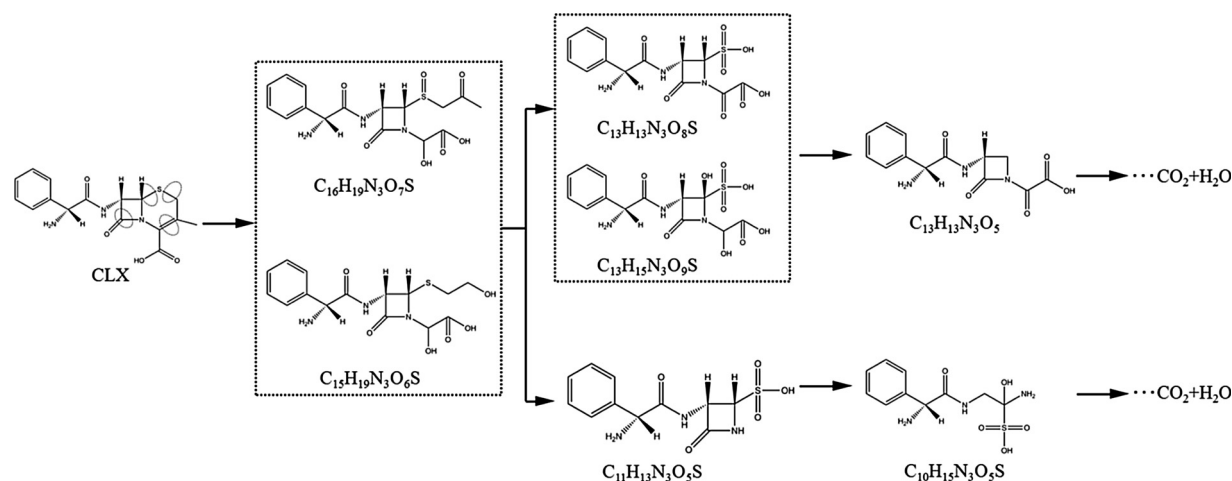


Fig. 8. Proposed degradation pathways of CLX by catalytic ozonation with $\text{MnO}_2\text{-NH}_2\text{-GO}$.

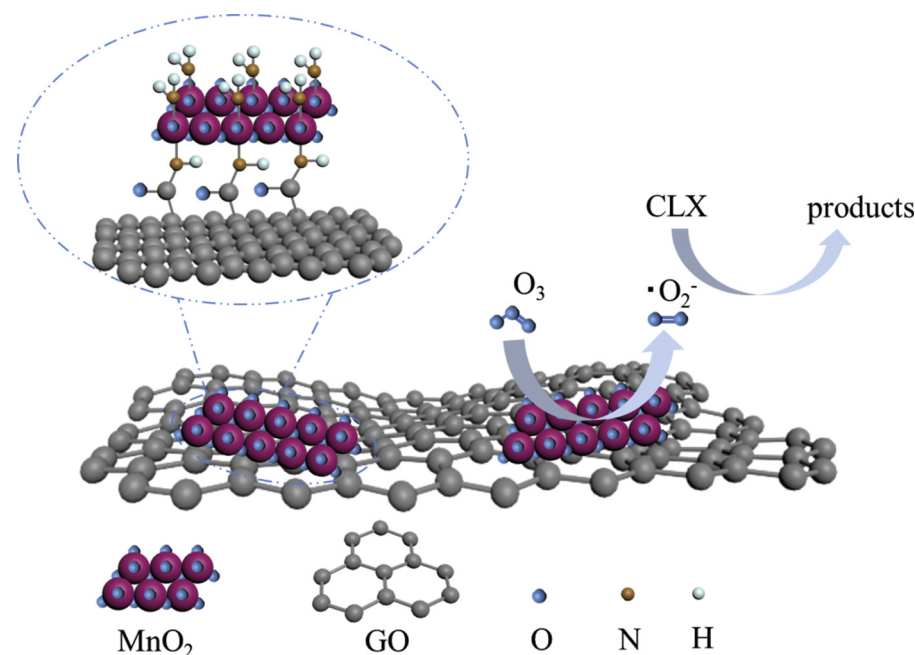


Fig. 9. Schematic diagram of the catalytic ozonation mechanism based on $\text{MnO}_2\text{-NH}_2\text{-GO}$.

relative content of Mn^{4+} increases from 46.3% to 52.1% calculated from the area ratios of Mn^{3+} and Mn^{4+} peaks, indicating the redox reaction between Mn^{3+} and Mn^{4+} is triggered by electron transfer proceeding in catalytic ozonation. Fig. 7c shows the XPS of Mn 2p region of $\text{MnO}_2\text{-NH}_2\text{-GO}$ after five times used for catalytic ozonation, in which the relative content of lattice Mn^{3+} decreases to 27.9% while the relative content of Mn^{4+} increases to 72.1%. Based on the results shown in Figs. 4–7, it can be concluded that the $\text{Mn}^{3+}/\text{Mn}^{4+}$ provide acid sites for ozone decomposition to generate $\cdot\text{O}_2^-$ radicals.

The degradation products of CLX by catalytic ozonation with $\text{MnO}_2\text{-NH}_2\text{-GO}$ were detected by HPLC-MS/MS analysis. The details of products with their mass spectrum and structure are shown in Figs. S6. During the catalytic ozonation, the bonds of $\text{C}=\text{C}$ on the nitrogen- and sulfur-containing heterocyclic of CLX are cleaved first to produce $\text{C}_{16}\text{H}_{19}\text{N}_3\text{O}_7\text{S}$ (P-397) and $\text{C}_{15}\text{H}_{19}\text{N}_3\text{O}_6\text{S}$ (P-369). With the degradation proceeding, two main competing reaction pathways are observed through the oxidation of two bonds, S-C and C-N of products molecule, which are illustrated in Fig. 8. The degradation process includes: (i) the cleavage of S-C bond in products, producing $\text{C}_{13}\text{H}_{13}\text{N}_3\text{O}_8\text{S}$ (P-371), $\text{C}_{13}\text{H}_{15}\text{N}_3\text{O}_9\text{S}$ (P-389) and $\text{C}_{13}\text{H}_{13}\text{N}_3\text{O}_5$ (P-291), and (ii) the

cleavage of C-N bond in products, generating $\text{C}_{11}\text{H}_{13}\text{N}_3\text{O}_5\text{S}$ (P-299) and $\text{C}_{10}\text{H}_{15}\text{N}_3\text{O}_5\text{S}$ (P-289). The intermediate products could be degraded and even mineralized during catalytic ozonation.

The mechanism of catalytic ozonation with $\text{MnO}_2\text{-NH}_2\text{-GO}$ is schematically shown in Fig. 9. The MnO_2 and GO are combined via amino, which tends to form covalent bonds with the manganese atom of MnO_2 and the oxygen-containing functional group of GO [43,44]. In the catalytic ozonation the $\text{Mn}^{3+}/\text{Mn}^{4+}$ serve as active sites for the dissolved ozone and provide electrons to molecular ozone, inducing ozone decomposition to generate radicals of $\cdot\text{O}_2^-$ [45]. The GO acts as the role to accelerate electron transfer and facilitate ozone decomposition for $\cdot\text{O}_2^-$ generation, resulting in an enhanced catalytic ozonation with higher removal efficiency of CLX.

4. Conclusions

A simple and smart catalyst of $\text{MnO}_2\text{-NH}_2\text{-GO}$ was designed and synthesized for catalytic ozonation to removal CLX from water. The hybrids of MnO_2 and GO ($\text{MnO}_2\text{-GO}$) are not strong enough to provide stable catalytic performance owing to their easy decoupling in catalytic

ozonation. The amino-functionalization enhances the bonding of MnO₂ and GO by the formation of covalent bonds bridged by amino groups between MnO₂ and oxygen groups of GO. The MnO₂-NH₂-GO shows much higher and more stable catalytic performance than MnO₂ or MnO₂-GO in the catalytic ozonation of CLX. The active radicals of ·O₂⁻ predominate the catalytic ozonation, and Mn³⁺/Mn⁴⁺ act as active sites for molecular ozone decomposition to generate radicals of ·O₂⁻ during the reaction process. This work gives an in-depth understanding of MnO₂-NH₂-GO and provides a catalyst with high performance and stability to ozonation for antibiotics removal from water or wastewater.

Notes

The authors declare no competing financial interest.

Acknowledgments

The authors greatly appreciate the financial supports from the National Key Research and Development Program of China (Grants 2016YFB0301800) and Public Welfare Project of the Science and Technology Department of Zhejiang Province (Grants 2015C33029).

Appendix A. Supplementary data

Supplementary material related to this article can be found, in the online version, at doi:<https://doi.org/10.1016/j.apcatb.2019.117797>.

References

- [1] X. Liu, J.C. Steele, X. Meng, Usage, residue, and human health risk of antibiotics in Chinese aquaculture: a review, *Environ. Pollut.* 223 (2017) 161–169.
- [2] I.T. Carvalho, L. Santos, Antibiotics in the aquatic environments: a review of the European scenario, *Environ. Int.* 94 (2016) 736–757.
- [3] K. Kümmerer, The presence of pharmaceuticals in the environment due to human use - present knowledge and future challenges, *J. Environ. Manage.* 90 (2009) 2354–2366.
- [4] J. Liu, M. Wong, Pharmaceuticals and personal care products (PPCPs): a review on environmental contamination in China, *Environ. Int.* 59 (2013) 208–224.
- [5] A. Christou, A. Agüera, J.M. Bayona, E. Cytryn, V. Fotopoulos, D. Lambropoulou, C.M. Manaia, C. Michael, M. Revitt, P. Schröder, D. Fatta-Kassinos, The potential implications of reclaimed wastewater reuse for irrigation on the agricultural environment: the knowns and unknowns of the fate of antibiotics and antibiotic resistant bacteria and resistance genes-A review, *Water Res.* 123 (2017) 448–467.
- [6] M.C. Dodd, H.E. Kohler, U. von Gunten, Oxidation of antibacterial compounds by ozone and hydroxyl radical: elimination of biological activity during aqueous ozonation processes, *Environ. Sci. Technol.* 43 (2009) 2498–2504.
- [7] K. Zhang, X. Zhou, P. Du, T. Zhang, M. Cai, P. Sun, C. Huang, Oxidation of β-lactam antibiotics by peracetic acid: reaction kinetics, product and pathway evaluation, *Water Res.* 123 (2017) 153–161.
- [8] J. Gomes, R. Costa, R.M. Quinta-Ferreira, R.C. Martins, Application of ozonation for pharmaceuticals and personal care products removal from water, *Sci. Total Environ.* 586 (2017) 265–283.
- [9] J. Wang, Z. Bai, Fe-based catalysts for heterogeneous catalytic ozonation of emerging contaminants in water and wastewater, *Chem. Eng. J.* 312 (2017) 79–98.
- [10] A. Lv, C. Hu, Y. Nie, J. Qu, Catalytic ozonation of toxic pollutants over magnetic cobalt-doped Fe₃O₄ suspensions, *Appl. Catal. B-Environ.* 117–118 (2012) 246–252.
- [11] X. Tan, Y. Wan, Y. Huang, C. He, Z. Zhang, Z. He, L. Hu, J. Zeng, D. Shu, Three-dimensional MnO₂ porous hollow microspheres for enhanced activity as ozonation catalysts in degradation of bisphenol A, *J. Hazard. Mater.* 321 (2017) 162–172.
- [12] M. Kermani, B. Kakavandi, M. Farzadkia, A. Esrafili, S.F. Jokandan, A. Shahsavani, Catalytic ozonation of high concentrations of catechol over TiO₂@Fe₃O₄ magnetic core-shell nanocatalyst: optimization, toxicity and degradation pathway studies, *J. Clean. Prod.* 192 (2018) 597–607.
- [13] F. Nawaz, H. Cao, Y. Xie, J. Xiao, Y. Chen, Z.A. Ghazi, Selection of active phase of MnO₂ for catalytic ozonation of 4-nitrophenol, *Chemosphere* 168 (2017) 1457–1466.
- [14] Y. Dong, K. Li, P. Jiang, G.L. Wang, H. Miao, J. Zhang, C. Zhang, Simple hydrothermal preparation of α-, β-, γ-MnO₂ and the phase sensitivity on catalytic ozonation, *RSC Adv.* 4 (2014) 39167–39173.
- [15] G. Li, Y. Lu, C. Lu, M. Zhu, C. Zhai, Y. Du, P. Yang, Efficient catalytic ozonation of bisphenol-A over reduced graphene oxide modified sea urchin-like α-MnO₂ architectures, *J. Hazard. Mater.* 294 (2015) 201–208.
- [16] G. Li, K. Li, A. Liu, P. Yang, Y. Du, M. Zhu, 3D flower-like β-MnO₂/reduced graphene oxide nanocomposites for catalytic ozonation of dichloroacetic acid, *Sci. Rep.* 7 (2017) 43643.
- [17] I. Forrez, M. Carballa, K. Verbeken, L. Vanhaecke, T. Ternes, N. Boon, W. Verstraete, Diclofenac oxidation by biogenic manganese oxides, *Environ. Sci. Technol.* 44 (2010) 3449–3454.
- [18] M. Sui, S. Xing, L. Sheng, S. Huang, H. Guo, Heterogeneous catalytic ozonation of ciprofloxacin in water with carbon nanotube supported manganese oxides as catalyst, *J. Hazard. Mater.* 227–228 (2012) 227–236.
- [19] F. Nawaz, Y. Xie, J. Xiao, H. Cao, Y. Li, D. Zhang, Insights into the mechanism of phenolic mixture degradation by catalytic ozonation with a mesoporous Fe₃O₄/MnO₂ composite, *RSC Adv.* 6 (2016) 29674–29684.
- [20] W. Guo, C. Yu, S. Li, Z. Wang, J. Yu, H. Huang, J. Qiu, Strategies and insights towards the intrinsic capacitive properties of MnO₂ for supercapacitors: challenges and perspectives, *Nano Energy* 57 (2019) 459–472.
- [21] S. Zhang, L. Wang, C. Liu, J. Luo, J. Crittenden, X. Liu, T. Cai, J. Yuan, Y. Pei, Y. Liu, Photocatalytic wastewater purification with simultaneous hydrogen production using MoS₂ QD-decorated hierarchical assembly of ZnIn₂S₄ on reduced graphene oxide photocatalyst, *Water Res.* 121 (2017) 11–19.
- [22] J. Azadmanjiri, V.K. Srivastava, P. Kumar, J. Wang, A. Yu, Graphene-supported 2D transition metal oxide heterostructures, *J. Mater. Chem. A Mater. Energy Sustain.* 6 (2018) 1359–1357.
- [23] L. Jothinathan, J. Hu, Kinetic evaluation of graphene oxide based heterogeneous catalytic ozonation for the removal of ibuprofen, *Water Res.* 134 (2018) 63–73.
- [24] R. Mao, X. Zhao, H. Lan, H. Liu, J. Qu, Graphene-modified Pd/C cathode and Pd/GAC particles for enhanced electrocatalytic removal of bromate in a continuous three-dimensional electrochemical reactor, *Water Res.* 77 (2015) 1–12.
- [25] Y. Wang, Y. Xie, H. Sun, J. Xiao, H. Cao, S. Wang, 2D/2D nano-hybrids of γ-MnO₂ on reduced graphene oxide for catalytic ozonation and coupling peroxyomonosulfate activation, *J. Hazard. Mater.* 301 (2016) 56–64.
- [26] M. Hu, K.S. Hui, K.N. Hui, Role of graphene in MnO₂/graphene composite for catalytic ozonation of gaseous toluene, *Chem. Eng. J.* 254 (2014) 237–244.
- [27] Y. Jiang, M. Wei, J. Feng, Y. Ma, S. Xiong, Enhancing the cycling stability of Na-ion batteries by bonding SnS₂ ultrafine nanocrystals on amino-functionalized graphene hybrid nanosheets, *Synth. Lect. Energy Environ. Technol. Sci. Soc.* 9 (2016) 1430–1438.
- [28] X. Meng, C. Yu, X. Song, J. Iocozzia, J. Hong, M. Rager, H. Jin, S. Wang, L. Huang, J. Qiu, Z. Lin, Scrutinizing defects and defect density of selenium-doped graphene for high-efficiency triiodide reduction in dye-sensitized solar cells, *Angew. Chem. Int. Ed.* 57 (17) (2018) 4682–4686.
- [29] I. Michael, L. Rizzo, C.S. McArdell, C.M. Manaia, C. Merlin, T. Schwartz, C. Dagot, D. Fatta-Kassinos, Urban wastewater treatment plants as hotspots for the release of antibiotics in the environment: a review, *Water Res.* 47 (2013) 957–995.
- [30] G. Zhu, J. Zhu, W. Jiang, Z. Zhang, J. Wang, Y. Zhu, Q. Zhang, Surface oxygen vacancy induced α-MnO₂ nanofiber for highly efficient ozone elimination, *Appl. Catal. B-Environ.* 209 (2017) 729–737.
- [31] C. Liu, L. Lin, Y. Cao, H. Liu, Y. Guo, X. Zhang, Amino-functionalized seeds-induced synthesis of encapsulated Pd@Silicalite-1 core-shell catalysts for size-selective hydrogenation, *Catal. Commun.* 109 (2018) 16–19.
- [32] F. Chen, N. Gupta, R.K. Behera, P.K. Rohatgi, Graphene-reinforced aluminum matrix composites: a review of synthesis methods and properties, *Jom-US.* 70 (2018) 837–845.
- [33] H. Zhang, X. Hu, Preparation of Fe₃O₄-rGO via a covalent chemical combination method and its catalytic performance on p-NP bioreduction, *J. Environ. Chem. Eng.* 5 (2017) 3348–3353.
- [34] Y. Ren, H. Zhang, H. An, Y. Zhao, J. Feng, L. Xue, T. Luan, Z. Fan, Catalytic ozonation of di-n-butyl phthalate degradation using manganese ferrite/reduced graphene oxide nanofiber as catalyst in the water, *J. Colloid Interf. Sci.* 526 (2018) 347–355.
- [35] D. Wang, X. Li, J. Chen, X. Tao, Enhanced photoelectrocatalytic activity of reduced graphene oxide/TiO₂ composite films for dye degradation, *Chem. Eng. J.* 198–199 (2012) 547–554.
- [36] L. Zhu, H. Li, Z. Liu, P. Xia, Y. Xie, D. Xiong, Synthesis of the 0D/3D CuO/ZnO heterojunction with enhanced photocatalytic activity, *J. Phys. Chem. C.* 122 (2018) 9531–9539.
- [37] H. Che, C. Liu, W. Hu, H. Hu, J. Li, J. Dou, W. Shi, C. Li, H. Dong, NGQD active sites as effective collectors of charge carriers for improving the photocatalytic performance of Z-scheme g-C₃N₄/Bi₂WO₆ heterojunctions, *Catal. Sci. Technol.* 8 (2018) 622–631.
- [38] T. Wang, Z. Huang, H. Miao, W. Ruan, X. Ji, F. Sun, M. Zhao, H. Ren, Insights into influencing factor, degradation mechanism and potential toxicity involved in aqueous ozonation of oxcarbazepine (CHEM46939R1), *Chemosphere* 201 (2018) 189–196.
- [39] J. Zhang, Y. Wu, L. Liu, Y. Lan, Rapid removal of p-chloronitrobenzene from aqueous solution by a combination of ozone with zero-valent zinc, *Sep. Purif. Technol.* 151 (2015) 318–323.
- [40] F. Nawaz, Y. Xie, H. Cao, J. Xiao, X. YueqiuWang, M. Zhang, F. Li, Duan, Catalytic ozonation of 4-nitrophenol over an mesoporous α-MnO₂ with resistance to leaching, *Catal. Today* 258 (2015) 595–601.
- [41] Y. Ren, Q. Dong, J. Feng, J. Ma, Q. Wen, M. Zhang, Magnetic porous ferrospinel NiFe₂O₄: a novel ozonation catalyst with strong catalytic property for degradation of di-n-butyl phthalate and convenient separation from water, *J. Colloid Interf. Sci.* 382 (2012) 90–96.
- [42] W. Li, Z. Qiang, T. Zhang, F. Cao, Kinetics and mechanism of pyruvic acid degradation by ozone in the presence of PdO/CeO₂, *Appl. Catal. B-Environ.* 113–114 (2012) 290–295.
- [43] A. Chakravarty, D. Sengupta, B. Basu, A. Mukherjee, G. De, MnO₂ nanowires anchored on amine functionalized graphite nanosheets: highly active and reusable catalyst for organic oxidation reactions, *RSC Adv.* 5 (2015) 92585–92595.
- [44] A. Chakravarty, K. Bhowmik, A. Mukherjee, G. De, Cu₂O nanoparticles anchored on amine-functionalized graphite nanosheet: a potential reusable catalyst, *Langmuir*. 31 (2015) 5210–5219.
- [45] P. Wei, D. Qin, J. Chen, Y. Li, M. Wen, Y. Ji, G. Li, T. An, Photocatalytic ozonation mechanism of gaseous n-hexane on MOx-TiO₂-foam nickel composite (M = Cu, Mn, Ag): unveiling the role of ·OH and ·O₂⁻, *Environ. Sci.-Nano.* 6 (2019) 959–969.